Electronic Supplementary Information (ESI) for

Towards controlled bubble nucleation in microreactors for enhanced mass transport

Renée M. Ripken,[a,b] Jeffery A. Wood,[c] Stefan Schlautmann,[b] Axel Guenther,[d] Han J.G.E. Gardeniers[b] and Séverine Le Gac[a†]

[a] Applied Microfluidics for BioEngineering Research, MESA+ Institute for Nanotechnology, TechMed Centre, University of Twente, P.O Box 217, 7500 AE, Enschede, The Netherlands

[b] Mesoscale Chemical Systems, MESA+ Institute for Nanotechnology, University of Twente, P.O Box 217, 7500 AE, Enschede, The Netherlands

[c] Soft Matter, Fluidics and Interfaces, MESA+ Institute for Nanotechnology, University of Twente, P.O Box 217, 7500 AE, Enschede, The Netherlands

[d] Guenther Laboratory, Mechanical and Industrial Engineering, University of Toronto, 5 King's College Road, Toronto, ON M5S 3G8, Canada

[†] *Corresponding author:* s.legac@utwente.nl, Phone: +31 53 4892722

SI.1 Dedicated chip-holder and microfluidic device

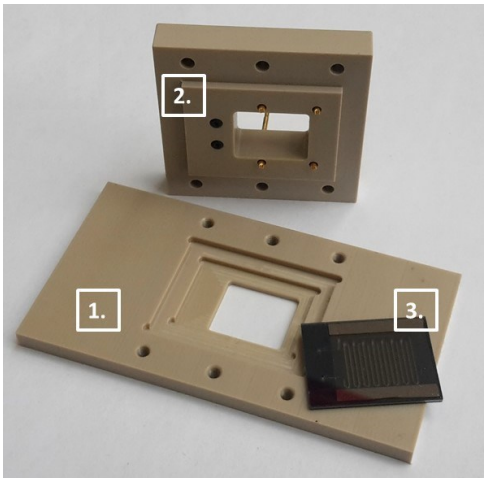

Figure S1: PEEK chip holder and microfluidic device, where the bottom plate (1.) has an optical window, and the top plate (2.), besides an optical window, has fluidic connections and pushpins. The microfluidic device (3.) is clamped between the two plates, the plates are tightened with screws (not shown).

SI.2 Geometry considered for the 3D COMSOL simulations

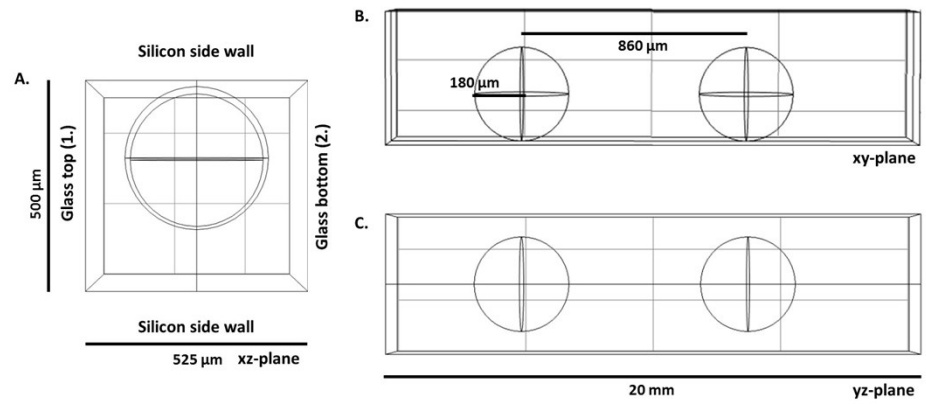

Figure S2. Geometry considered in the 3D COMSOL simulations from 3 different perspectives, xz-plane, *i.e.*, view through the channel in the flow direction (A.), xy-plane, *i.e.*, a sideview of the microchannel (B.) and yz-plane, *i.e.*, the channel in top view (C.) The flow in (B) and (C) is from left to right.

SI.3 Micropit activity and temperature homogeneity

The glass layer containing the micropits was evaluated before the 3-layered microfluidic device was assembled. The glass layer was submerged in a supersaturated CO_2/water mixture, after which pressure reduction leads to bubble nucleation. The bubbles formed on the micropits, and the resulting pattern was consistent with the meandering design. A bubble departure radius of 223 µm was predicted for a 1-µm radius micropit using Equation 1, with 1.324 $kg.m^{-3}$ and 998.20 $kg.m^{-3}$ the density of air and water at 20 °C (worst case scenario),[18, 19] respectively, and $7.28x10^{-2}$ $N.m^{-1}$ the surface tension of air/water at 20°C (worst case scenario),[20] and 9.81 $m.s^{-2}$ the gravitational constant. This predicted bubble departure size is smaller than the hydraulic diameter of the channel (512 µm), so that bubbles should not block fluid flow.

The heating functionality as well as the homogeneity of the temperature field of the ITO layer with Pt-contacts was evaluated with an IR-camera, demonstrating a homogeneous field at 266 °C.

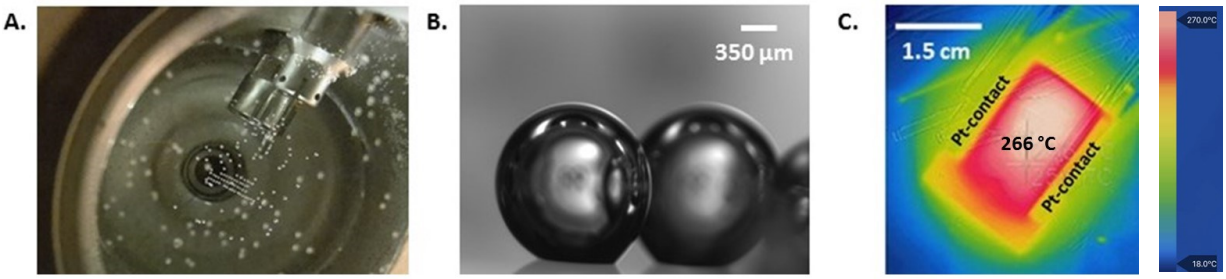

Figure S3. Bubble nucleation in a supersaturated CO_2/water mixture on a glass substrate containing only the hydrophobic pits, observed from the top (A) and side (B). The bubbles were generated along the meandering pattern formed by the hydrophobic pits etched in the glass substrate. C. ITO heater, thermal image (IR camera), with red/white indicating a temperature of 266 °C, whereas the surroundings in blue were at room temperature. This image indicated a homogeneous temperature field between the electrodes

SI.4 Microfluidic device calibration

After assembling the 3-layered stack, the microfluidic devices were calibrated for current, power and, most importantly, temperature as a function of the applied voltage. An external power supply was applied to the pushpin connections touching the Pt-contacts of the device and the voltage was increased in steps of 1 or 2 V, starting from 5 V. From the graphs for current and power in Figure 4, an estimated resistance of 60-85 Ohm was determined. These graphs also demonstrate that the electric properties varied between the multiple devices, likely due to the fabrication process, suggesting, for example, a non-uniform ITO layer. As ITO was sputtered device by device, variations in the ITO layer could have occurred between the samples. Therefore, every individual device must be calibrated before use.

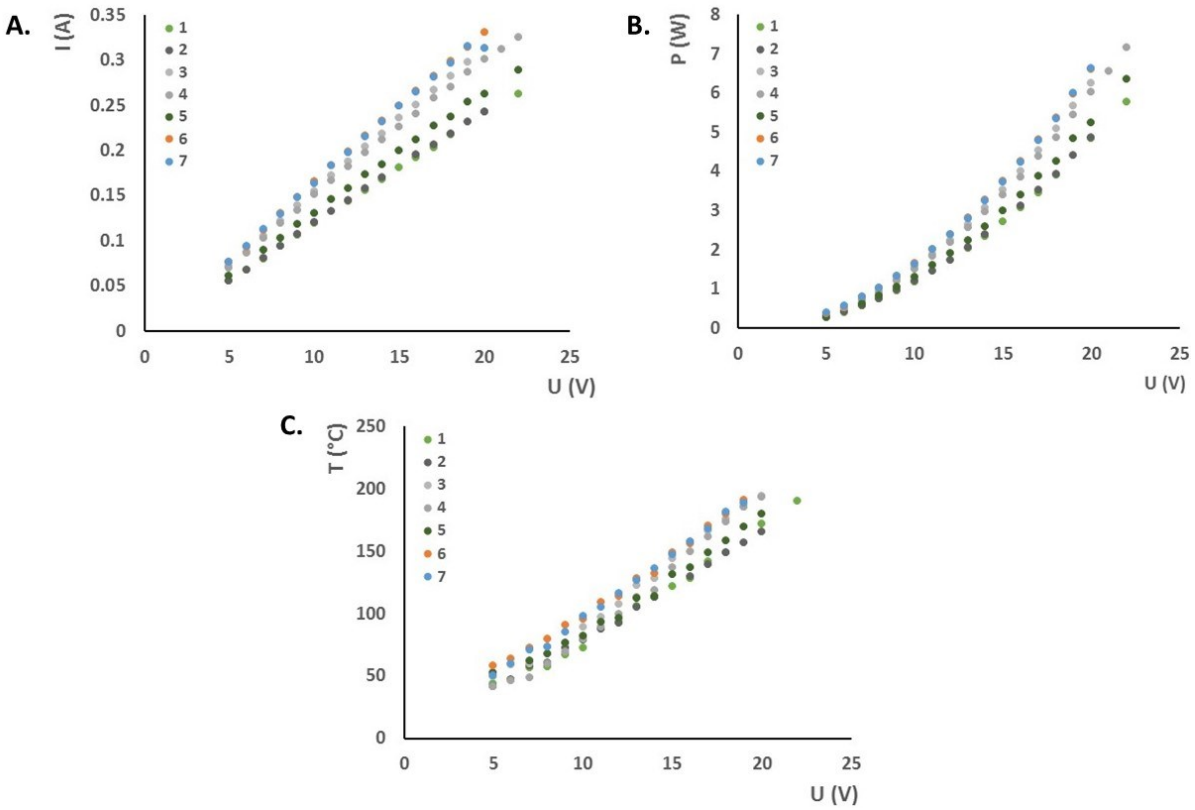

Figure S4. Calibration of the integrated ITO-heater: Recorded current (A.), power (B.) and temperature (C.) as a function of the applied voltage to the Pt-contacts on 7 different microfluidic devices placed in the chip holder.

SI.5 Formation of large slugs at the device inlet

Larger slugs also often formed at the inlet of the device (Figure S3), indicating that outgassing occurred as soon as the cold liquid came in contact with the heated device.

Figure S5. Outgassing occurring at the channel inlet: Large CO_2 bubbles already forming at the inlet of the device (bottom left of the figure).

SI.6 Deactivation of the micropits

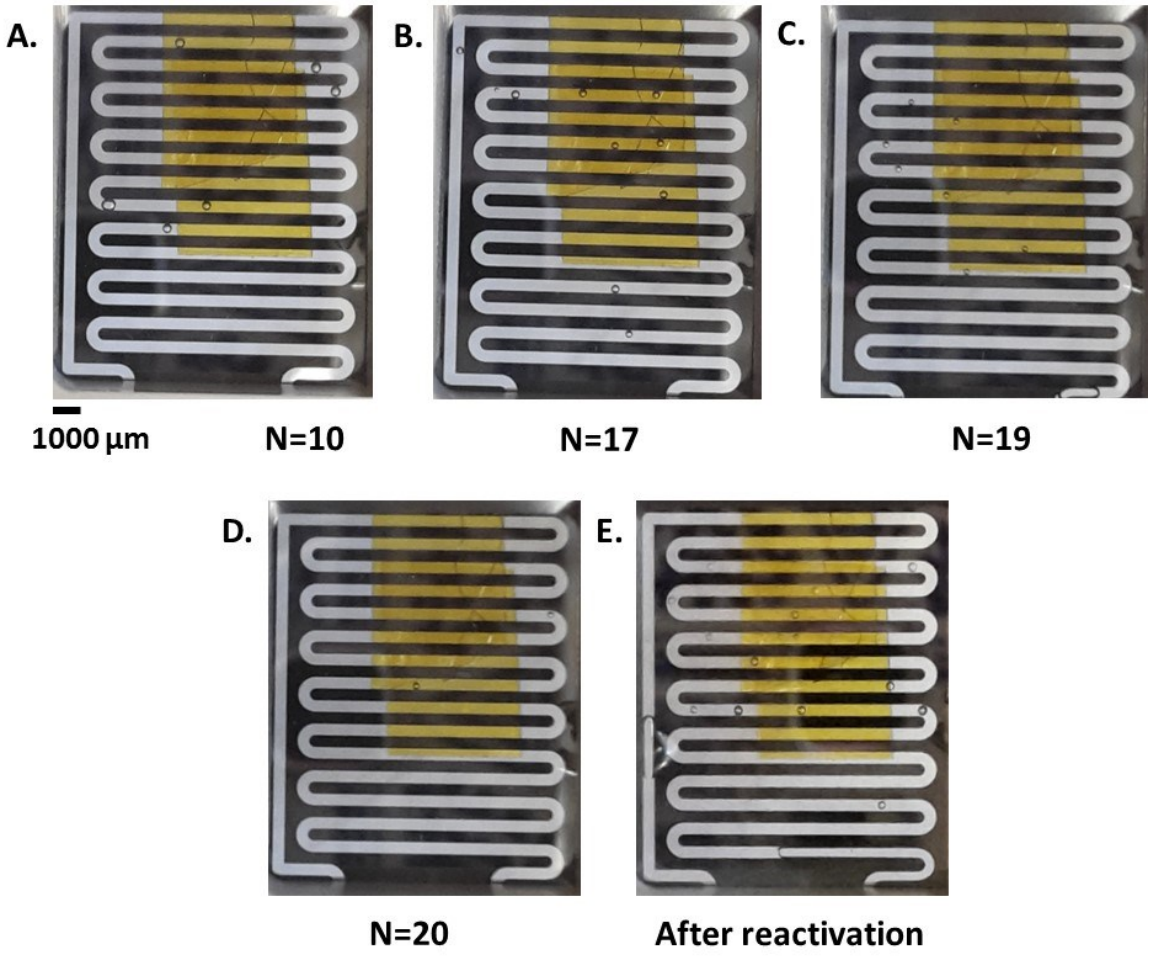

Figure S6. Micropit deactivation and reactivation, N being the number of nucleation cycles. After about 20 cycles (D), almost no nucleation was observed. The micropits were successfully reactivated by heating for 45 minutes at 175 °C (E).

SI. 7 SEM images of the micropit and scallop defects

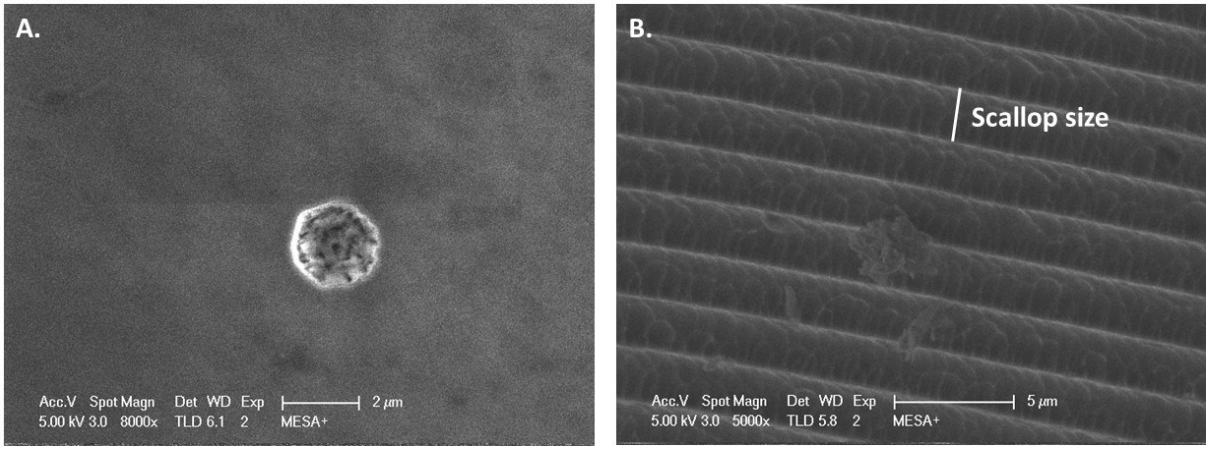

Figure S7. SEM images of a hydrophobic micropit etched in glass (A.) and etching scallops (B.). Both structures were roughly 2-µm in size.